4838 *Biochemistry* **2009,** *48,* 4838–4845
DOI: 10.1021/bi900166y

BIOCHEMISTRY
including biophysical chemistry & molecular biology
*Article*

# Crystal Structure of the Human Lymphoid Tyrosine Phosphatase Catalytic Domain: Insights into Redox Regulation[†,‡]

Sophia J. Tsai,[§,⊥] Udayaditya Sen,[§,⊥] Lei Zhao,[∥] William B. Greenleaf,[§] Jhimli Dasgupta,[§] Edoardo Fiorillo,[∥] Valeria Orrú,[∥] Nunzio Bottini,*[,∥] and Xiaojiang S. Chen*[,§]

[§]*Molecular and Computational Biology, University of Southern California, Los Angeles, California 90089, and* [∥]*The Institute for Genetic Medicine, University of Southern California, Los Angeles, California 90033* [⊥]*These authors contributed equally*

*Received February 2, 2009; Revised Manuscript Received April 16, 2009*

ABSTRACT: The lymphoid tyrosine phosphatase (LYP), encoded by the PTPN22 gene, recently emerged as an important risk factor and drug target for human autoimmunity. Here we solved the structure of the catalytic domain of LYP, which revealed noticeable differences with previously published structures. The active center with a semi-closed conformation binds a phosphate ion, which may represent an intermediate conformation after dephosphorylation of the substrate but before release of the phosphate product. The structure also revealed an unusual disulfide bond formed between the catalytic Cys and one of the two Cys residues nearby, which is not observed in previously determined structures. Our structural and mutagenesis data suggest that the disulfide bond may play a role in protecting the enzyme from irreversible oxidation. Surprisingly, we found that the two noncatalytic Cys around the active center exert an opposite yin-yang regulation on the catalytic Cys activity. These detailed structural and functional characterizations have provided new insights into autoregulatory mechanisms of LYP function.

Regulating tyrosine phosphorylation level is a fundamental mechanism for numerous important aspects of eukaryote physiology, as well as human health and disease (*1*−*3*). Cellular tyrosine phosphorylation levels are regulated by the antagonistic activities of two classes of enzymes, the protein tyrosine kinases (PTKs)[1] and the protein tyrosine phosphatases (PTPs). Recent findings have led to the emerging recognition that PTPs play specific and even dominant roles in setting the levels of tyrosine phosphorylation in cells and in the regulation of many physiological processes (*2*−*7*). Disruption of the equilibrium maintained by PTPs and PTKs causes a range of human disease, including cancer, diabetes, and autoimmunity (*8*−*16*).

A major class of PTPs, known as classical PTPs, include transmembrane PTPs and nonreceptor PTPs (NRPTP), which are then further subclassified based on their sequence similarities and noncatalytic domain structural motifs (*4*, *8*). NRPTPs display various intracellular localizations, determined by amino acid sequences outside the catalytic domain. The lymphoid-specific tyrosine phosphatase (LYP) encoded by the PTPN22 gene is a classical NRPTP (belonging to the NT4 subfamily), expressed exclusively in cells of hematopoietic origin. LYP, an intracellular 105 kDa protein that contains two distinct functional domains, acts as an inhibitor to downregulate T-cell activation (*17*) by dephosphorylating lymphocyte receptor tyrosine kinases (SRC family). The N-terminal portion of LYP contains a single tyrosine phosphatase catalytic domain, and the noncatalytic C-terminal region contains four proline-rich SH3 domains.

The importance of LYP in immune system regulation has been recently demonstrated by the finding that a human variant W620, caused by a single nucleotide polymorphism in PTPN22 at nucleotide 1858, leads to a significantly increased risk for autoimmune diseases including type-1 diabetes, rheumatoid arthritis, and systemic lupus erythematosus (*11*, *16*, *18*, *19*). Since the autoimmune-predisposing LYP-W620 variant is a gain-of-function mutation and shows increased phosphatase activity (*20*), LYP is currently considered a promising drug target for autoimmunity. Elucidation of the structure and regulation of LYP is important in order to understand its mechanism of action in autoimmunity and to develop innovative approaches to the pharmacological inhibition of the enzyme for therapeutic purposes.

One possible mechanism of regulating cysteine-based PTP activity is through oxidation of the catalytic cysteine (Cys). PTPs are differentially oxidized and inactivated *in vitro* and in living

[†]This work is supported in part by the National Institutes of Health grants (AI070544 and AI0559926).

[‡]The coordinates and structure factors for the disulfide structure of PTPN22 (PDB ID 3H2X) have been deposited in the Protein Data Bank.

*To whom correspondence should be addressed. N.B.: e-mail, nunzio@usc.edu. X.S.C.: e-mail, xiaojiang.chen@usc.edu; tel, 213-740-5487; fax, 213-740-4390.

[1]Abbreviations: PTKs, protein tyrosine kinases; PTPs, protein tyrosine phosphatases; NRPTP, nonreceptor PTPs; LYP, lymphoid-specific tyrosine phosphatase; Cys, cysteine; ROS, reactive oxygen species; LYPcat, catalytic domain of LYP; catC227, catalytic cysteine; DiFMUP, 6,8-difluoro-4-methylumbelliferyl phosphate; pTyr, phospho-tyrosine.

 Published on Web 04/16/2009 

cells. Many stimuli, including growth factors, cytokines, and ultraviolet light, induce the production of reactive oxygen species (ROS) capable of shifting the cellular redox state toward oxidation. Oxidation of the active site Cys, a soft target because of its low p$K_a$, abrogates its nucleophilic properties and inactivates the enzyme. There has been accumulating evidence that at least part of the cellular responses to these stimuli are due to the specific and transient inactivation of the PTPs (*21*, *22*), indicating that PTPs are important sensors of the cellular redox state and that oxidation of PTPs is emerging as an important regulatory mechanism.

Thus far, three mechanisms have described the redox regulation in the PTP superfamily. One mechanism involves a disulfide bridge formation between the catalytic Cys and a second Cys found within the signature motif followed by reactivation through reduction of the catalytic Cys. This method of protecting the active site Cys has been shown in the low molecular weight protein tyrosine phosphatase (*23*−*25*). Another similar mechanism involving disulfide formation is seen in PTEN and Cdc25 (*12*, *26*−*29*). Third, the redox mechanism seen in classical PTPs involves the formation of a reversible sulfenamide ring by the catalytic Cys with the main-chain amide of the next residue, namely, serine, within the signature motif and thereby protecting the catalytic Cys from damage by ROS. This type of mechanism has been previously described in PTP-1B (*30*, *31*).

In this paper, we describe the crystal structure of the catalytic domain of LYP (named here as LYPcat) that has a bound phosphate ion at the active site and has a semi-closed conformation for the active site loop. The active site of LYP consists of a catalytic Cys residue that is within bonding distance of two additional Cys around the active center in the 3-D structure, which is unique to the LYP subfamily. The structure reveals a disulfide bond not previously seen in classical PTPs between the catalytic Cys (catC227) and the Cys residue (C129) outside the signature motif (or back-door Cys) that is conserved only in LYP and its close homologues, PTP-PEST and BDP1. We also found that a secondary P-loop Cys (C231) may function as a negative regulator of LYP activity. Our structural and mutational data suggest that in LYPcat the two noncatalytic Cys around the active center may play an important yin-yang regulatory role on the enzyme activity, possibly through redox reactions to influence the catalytic Cys.

## EXPERIMENTAL PROCEDURES

*Reagents*. Hydrogen peroxide ($H_2O_2$; VWR) was freshly diluted from the stock solution. PTP activity was assayed using 6,8-difluoro-4-methylumbelliferyl phosphate (DiFMUP; Invitrogen) as the substrate.

*Cloning, Expression, and Purification*. LYPcat (residues 2−309) was cloned into the pET28a expression vector and sequenced. The transformed vector was expressed in *Escherichia coli* BL21(DE3) cells. Expression was induced with 0.2 mM isopropyl 1-thio-$\beta$-D-galactopyranoside, and the cells were grown overnight at 25 °C. Cells were harvested by centrifugation and resuspended in 50 mM Tris-HCl, pH 8.0, 300 mM NaCl, and 5 mM $\beta$-mercaptoethanol. Cells were lysed by a microfluidizer and then centrifuged at 13000*g*. The His-tagged protein was purified using a $Ni^{2+}$ affinity column (Qiagen) following standard protocols. The resin was incubated overnight with 50 units of thrombin to remove the His tag. The eluted protein was further purified by gel filtration using a Superdex-75 column (GE Life Sciences). The purity and integrity of the protein were checked by SDS−PAGE. The eluted protein was concentrated to 18 mg/mL for crystallization experiments.

Mutants were prepared using the QuikChange protocol (Stratagene) and confirmed by DNA sequencing. Procedures for purification of all mutants were the same as those described for wild-type LYP.

*Crystallization and Data Collection*. Crystals of LYPcat were obtained using the hanging drop vapor diffusion method at 18 °C using a precipitant containing 2.0 M ammonium sulfate and 0.2 M sodium−potassium phosphate in 0.1 M MES, pH 6.2. Plate-shaped crystals were flash frozen after a quick soaking in a cryosolution containing 10% glycerol, 2.0 M ammonium sulfate, and 0.2 M sodium/potassium phosphate phosphate in 0.1 M MES, pH 6.2, and diffraction data up to 2.2 Å were collected at an in-house R-AXIS IV++ image plate (Rigaku). The data were processed using HKL2000, and data statistics are shown in Table 1.

*Structure Determination and Refinement*. The structure of LYPcat was initially solved by the molecular replacement method (AMoRe, CCP4 suite)(*32*), using the crystal structure of human protein tyrosine phosphatase receptor type J (PTPRJ; PDB ID 2CFV) as a search model with the closest sequence similarity to LYP available in the data bank at the time. Since PTPRJ has a low sequence identity (39%) with LYPcat, a polyalanine model was used in finding the solution. The solution was refined by rigid body and positional refinement, and the electron density map was calculated with CNS and displayed on Linux-based workstations using "O". The previously removed helices, loops, and the side chains were gradually added to the model, guided by the electron density map, and the model was refined using the standard slow-cool and positional refinement protocols of the CNS package using the data between 20 and 2.2 Å. The free *R* value was calculated throughout by randomly selecting 7% of the data as the test set. Inclusions of

Table 1: Crystallographic Statistics[a]

| | |
|---|---|
| **Crystal Cell Parameters** | |
| space group | $P2_1$ |
| cell dimensions | |
| *a*, *b*, *c* (Å) | 42.5, 68.9, 58.7 |
| $\beta$ (deg) | 101.6 |
| **Data Collection Statistics** | |
| resolution range (Å) | 50.0−2.2 |
| observations | 71791 |
| unique reflections | 16800 |
| completeness (%) | 99.2 (92.2) |
| $R_{sym}$ (%) (last bin) | 6.5 (26.9) |
| $I/\sigma$ (last bin) | 19.1 (5.5) |
| **Refinement Statistics** | |
| $R_{cryst}$ (%) | 17.6 |
| $R_{free}$ (%) | 20.4 |
| rms deviation | |
| bond length (Å) | 0.006 |
| bond angle (deg) | 1.6 |
| average *B* factor (Å$^2$) | 27.9 |

[a] $R_{sym} = \sum_{ij}|I_i(j) - \langle I(j)\rangle|/\sum_{ij}I_i(j)$, where $I_i(j)$ is the *i*th measurement of reflection *j* and $\langle I(j)\rangle$ is the overall weighted mean of *i* measurements. $R_{cryst} = \sum_{hkl}||F_o| - |F_c||/\sum_{hkl}|F_o|$; 7% of the reflections were excluded for the $R_{free}$ calculation.

side chains, water molecules, and the bound phosphate ion coupled with a few cycles of refinement yielded good refinement statistics (Table 1).

*PTP Activity Assay*. The PTP activity of the purified LYPcat was assayed in a 96-well plate in a total volume of 100 $\mu$L, containing 0.05 M Tris-HCl, pH 7.4, 0.05 $\mu$M wild type and C129S mutant, 0.15 $\mu$M C231S and C129S−C231S mutants, and 0.1 mM DiFMUP. In order to compare each assay to a fully active enzyme, controls were reactivated with 10 mM dithiothreitol (DTT) for 15 min before the assay. Inactivation was achieved by oxidation through incubation with 1.0 mM $H_2O_2$ for 10 min. Reactivation of oxidized wild type and mutants was achieved by incubation of the inactivated enzymes with 10 mM DTT for 15 min. All incubations were performed at 25 °C and data recording at 37 °C in a Wallac Victor Microplate Reader (PerkinElmer). The DiFMUP fluorescence signal was measured at an excitation of 355 nm and an emission of 460 nm in the microplate reader approximately one time per minute for 8 min to assess linearity of the reaction.

*Calculations of Specific Activity and Percent Reactivation*. Calculations of specific activity were done by creating a standard curve of varying concentrations of DiFMU, to get the rate of product formation. This rate was then divided by protein concentration and time to get specific activity. To get the percent of reactivation using DTT after inactivation of the enzyme by $H_2O_2$, the reactivated activity of each mutant was divided by its full activity before inactivation.

*Statistics*. To check for statistical significance, *p*-values for the paired *t* test were calculated using the GraphPad QuickCalcs Web site: http://www.graphpad.com/quickcalcs/ttest1.cfm (accessed September 2008).

## RESULTS AND DISCUSSION

*Crystal Structure Determination*. LYPcat (residues 2−309 of LYP) crystallizes in the spacegroup $P2_1$ with one molecule in the asymmetric unit. The three-dimensional structure of LYPcat has been refined to a crystallographic *R*-factor of 17.6% ($R_{free}$ 20.4%), and the accuracy of the refined model is consistent with the quality of the diffraction data (Table 1). The $2F_o - F_c$ map for the entire polypeptide chain is well-defined except for the N-terminal His tag and a few C-terminal residues (303−309). Unambiguous electron densities are observed for all surface loops (Figure 1A), including the PTP signature motif that forms the catalytic pocket (P-loop, residues 226−233), the pTyr recognition loop (confers specificity to pTyr, residues 54−60), the WPD loop (contains the general acid−base catalyst D195, residues 193−204), and the Q-loop (contains the conserved Q274 required to position and activate a water molecule for nucleophilic attack, residues 274−301) (Figures 1A and 2B).

Overall, our structure is similar to the previously published LYP structures (*33*, *34*); however, noticeable differences in some important loops are noticed. While the pTyr recognition loop, Q-loop, and P-loop appear unchanged, the WPD loop around the active center shows an ~8 Å difference between the open and closed states in the various structures. In our structure, the WPD loop appears to be in an intermediary stage between open and closed forms (Figure 1B−D; see also below). In addition to the changes noted in the major surface loops, we can see differences in the LYP-specific loop at the end of helix α2′, which, as noted previously, takes on different conformations depending on the binding state of the protein (*33*). Moreover, a disulfide bond between catC227 and C129 is observed in our structure, which is not present in the previously reported structures (*33*, *34*).

*Catalytic Pocket of LYPcat*. The phosphotyrosine binding site is a deep pocket on the surface of LYPcat. Electrostatic potential calculation shows that the bottom of the phosphotyrosine binding pocket has a strong positive charge (Figure 2A). Interestingly, a clear electron density corresponding to a phosphate ion is observed in this active site cleft of our structure (Figure 2C). The detailed interactions between the bound phosphate, which could mimic the substrate/product of PTP, and the P-loop (Figure 3) are discussed below. While primary sequence alignments and structures of other PTP superfamily members have just one Cys residue close to the catalytic Cys, our LYPcat structure reveals two Cys residues, C129 and C231, in the vicinity of the catalytic C227 (catC227). Sequence alignments with other classical PTPs reveal that these Cys are highly conserved in LYP and its close homologues PTP-PEST and BDP1, all of which belong to the NT4 subfamily (Figure 2B). The residue corresponding to C129 is strictly threonine or asparagine in other classical human PTPs, and the residue corresponding to C231 is mostly threonine or valine (*9*). In our structure, a disulfide bond is formed between catC227 and C129, which is in a reduced state in previously reported structures (*33*, *34*). This disulfide bond formation is not feasible in other classical PTPs due to the lack of the equivalent Cys residue. C129 in our structure is spatially close enough to catC227 to make the disulfide bond, although it is relatively distant by primary sequence (Figure 2B,C). This arrangement is known in other PTP classes as a back-door Cys (*12*, *29*).

*Movement of the WPD Loop*. WPD loop movement has been shown to be important in PTP substrate binding. The WPD loop of the structure in this report is in a semi-closed state (Figure 1C,D). The disulfide bond observed between catC227-C129 restricts movement of the β3-β4 loop, preventing full closure of the WPD loop over the active site. In addition, the strong stacking interaction between W193 of the WPD loop and the guanidinium group of R233 in the P-loop observed in our structure (Figure 3A) must be broken, as seen in closed-form structures in the LYP-apo and tungstate-bound PTP-1B (PDB IDs 2P6X and 2NHQ), before the WPD loop can move close enough for phosphatase activity to begin. The interaction of W193 and the invariant R233 found in the P-loop plays an important role in the closure of the WPD loop (*9*). In our structure of LYPcat, R233 adopts an extended conformation and is engaged in a strong stacking interaction with W193 of the conserved WPD loop. The conformation of the R233 side chain is further stabilized by a salt-bridge interaction with conserved E133 (Figure 3A). This position of the R233 side chain allows room for the disulfide bond formation between the catalytic C227 and C129 (Figures 2C and 3A), a residue highly conserved only in PEST-enriched phosphatases (Figure 2B). As a result, the catC227 Sγ is not facing the phosphate ion in our structure.

*Phosphate at the Catalytic Site*. From the early stages of structural refinement, a well-ordered, tetrahedral-shaped density was observed near the P-loop and catC227 (Figure 2A, C). Although both ammonium sulfate and potassium phosphate were present in the crystallization mother liquor, the tetrahedral densities were assigned as phosphate ions, in accordance with the phosphatase activity of the protein. The phosphate ion is well-defined with strong electron density and low *B* factors (Figure 2C). The oxygen atoms of the phosphate ion interact with the backbone amide nitrogen atoms of the residues

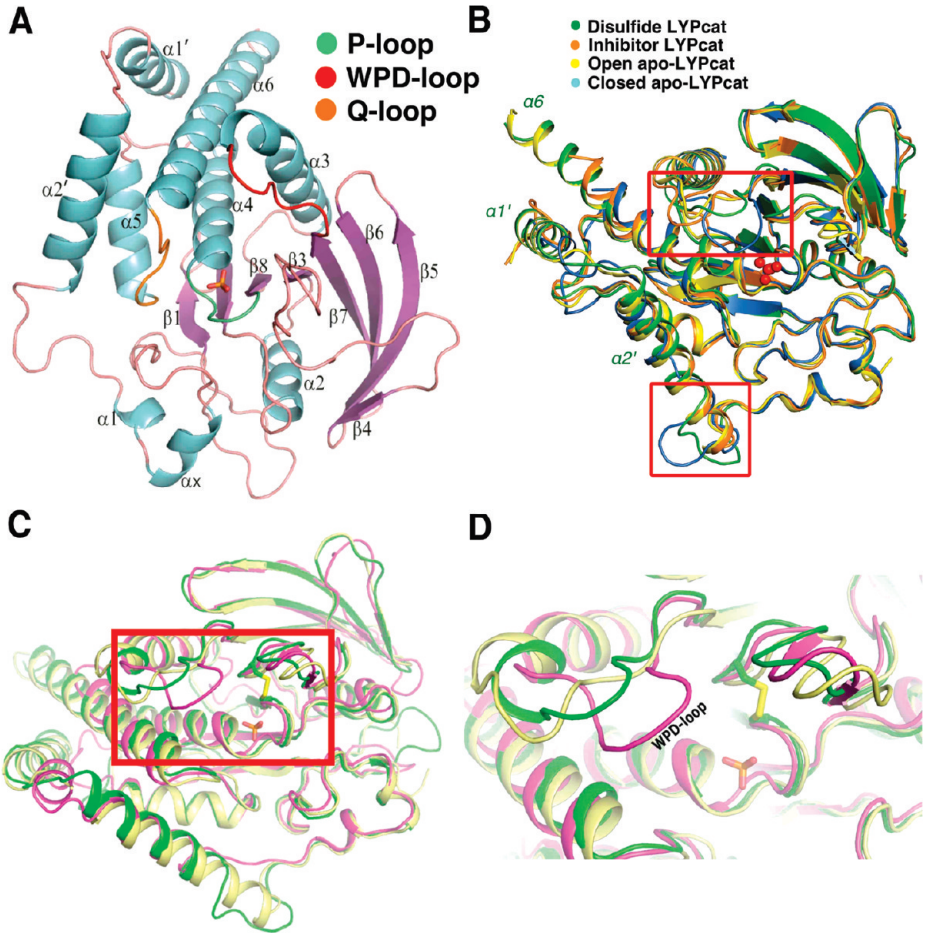


FIGURE 1: LYP structure and comparison to other PTPs. (A) Ribbon diagram of LYP catalytic domain (LTPcat). α-Helices are in blue, β-sheets are colored purple, the P-loop is colored green, the WPD loop is in red, the Q-loop is in orange, and all other loops are in pink. The bound phosphate ion at the active site is shown as a stick model. (B) Superposition of known structures of LYPcat, with the major areas of differences in surface loops indicated by the red boxes. The structure in this report is shown in green, LYPcat with an inhibitor (PDB code 2QCT) is in orange, the corresponding structure without inhibitor (PDB code 2QCJ) is in blue, and the LYPcat alone with the PDB code 2P6X is in yellow. The phosphate ion is shown in red ball and stick representation. (C) Comparison of the different WPD loop conformations between LYPcat (shown in green), non-phosphate-bound LYPcat (in yellow, PDB code 2P6X), and the tungstate-bound PTP1B (in magenta, PDB code 2HNQ). The phosphate ion and disulfide bond of LYPcat are shown as sticks. (D) Zoomed view of the boxed area in panel C, showing different locations of the WPD loop in the three structures.

belonging to the P-loop (Figure 3A), and its position matches well with that of the tungstate ion, coordinated by the PTP-1B P-loop (PDB code 2HNQ) (Figure 3B). However, no hydrogen bond between the phosphate ion and the guanidinium nitrogen atoms of the signature motif arginine (R233) is observed in LYPcat, although it is weakly present in tungstate-bound PTP-1B. The series of structures of Cdc25B solved by Buhrman et al. (*12*) revealed a disulfide bond of the catalytic Cys with a back-door Cys (PDB code 1YS0). However, in this structure, the P-loop of Cdc25B has folded over the catalytic Cys like a lid, preventing access of the substrate to the catalytic pocket. When this structure is compared to the sulfate-bound Cdc25B structure (PDB entry 1QB0), they find that the main chain of the P-loop of the disulfide formed structure occupies the same location as the sulfate ion. It is suggested that this conformational change in the P-loop of the Cdc25B disulfide structure is to allow room for the disulfide bond to form, since steric restraints prevent the movement of the WPD loop and the active site arginine (*35*). In comparison, the P-loop of LYPcat is much more similar to the sulfate-bound structure of Cdc25B (*36*), with the catalytic pocket accessible to substrate. Thus, the WPD loop and active site arginine in LYPcat are presumably able to move in response to disulfide bond formation and do not require the movement of the P-loop to compensate. Buhrman et al. note that the catalytic Cys in their structure is not able to bind substrate without significant conformational rearrangement by breaking the disulfide bond.

*Novel Mechanism of Redox Regulation of LYP Activity.* The presence of an extra Cys in the P-loop and the participation of the back-door Cys in the disulfide bond as revealed in this structure suggest a potential function for protecting the essential catalytic Cys from oxidative damage, while also regulating the activity of LYPcat. The catalytic Cys of PTPs is known to be highly reactive to phosphotyrosines and highly susceptible to $H_2O_2$ oxidation (*26*) due to its microenvironment and its low $pK_a$ (4.7−5.4) (*37*). Oxidation of the essential Cys prevents enzymatic dephosphorylation because catalysis involves a covalently bound phospho-Cys intermediate that cannot form if the Cys has been oxidized. Under relatively mild oxidation conditions, this oxidation to sulfenic acid (Cys-SOH) is reversible through reduction by thiols. Highly oxidizing conditions lead to the irreversibly oxidized sulfinic acid (Cys-$SO_2$) and sulfonic acid (Cys-$SO_3$) states, which completely inactivate PTPs. Thus far, PTPs have shown three different methods of protection from $H_2O_2$ oxidation: classical PTPs form sulfenylamide rings with the neighboring amide from the main chain of the serine in the P-loop (*21*, *30*, *31*, *38*); Cdc25, VHR, and PTEN form disulfides with a

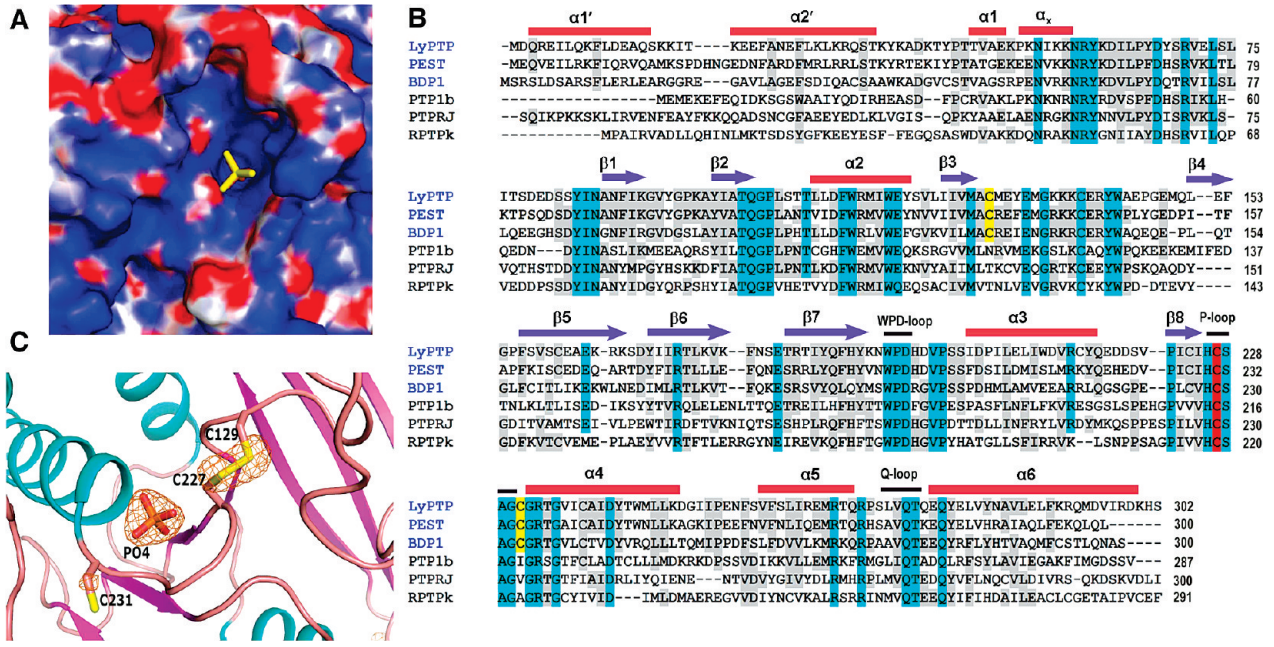


FIGURE 2: Binding of phosphate ion in the active site of LYPcat and sequence alignment. (A) Surface electrostatic potential of phosphate-bound LYPcat; the phosphate ion (in yellow) is located in a deep cleft of the surface. (B) Sequence and secondary structure alignment of LYPcat with other members of the NT4 subfamily and PTP-1B, PTPRJ, and RPTP$\kappa$. Blue arrows represent $\beta$-strands, red bars denote α-helices, and black lines denote catalytically important loops. The catalytic cysteine is highlighted in red, and the two other cysteines around the catalytic site are highlighted in yellow. Residues conserved in all of the sequences are highlighted in cyan, and those showing at least 50% conservation are in gray. The names of the NT4 subfamily are given in blue. (C) $F_o - F_c$ map is shown around the phosphate ion and disulfide bridge at a contour level of 4.5$\sigma$. The map was calculated where these atoms were omitted from the final coordinates. α-Helices are denoted in cyan, $\beta$-sheets are seen in purple, and loops are colored pink.

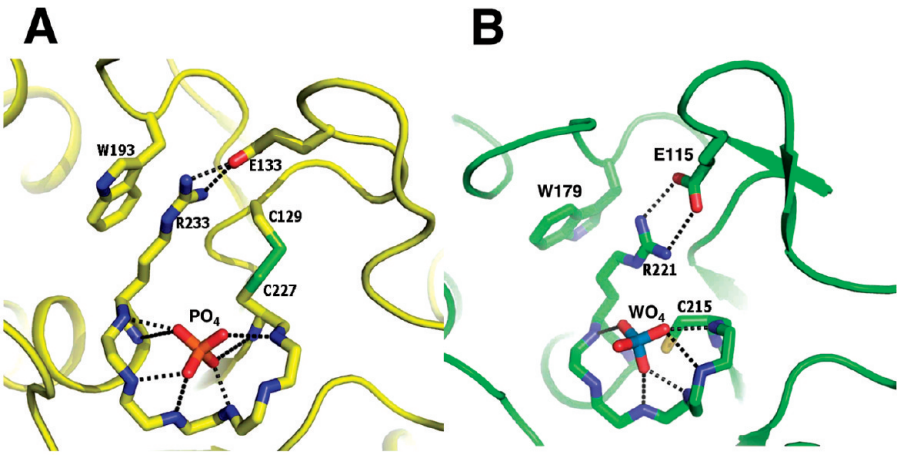


FIGURE 3: Active site geometries of PTPs. (A) Hydrogen bonds made by the active site phosphate ion in LYPcat with the amide nitrogen of the P-loop residues C227, S228, G230, C231, G232, and T234 and the interactions of R233 with W193 and E133. Side chains of residues 228−232 were omitted for clarity. (B) Interactions made by the active site tungstate ion with PTP-1B (coordinates taken from the PDB code 2HNQ); residues corresponding to R233, W193, and E233 are shown for comparison.

back-door Cys outside of the P-loop (*12*, *13*, *27*−*29*, *39*, *40*); and the low molecular weight PTP forms a disulfide with a Cys found within the P-loop (*23*, *41*). Interestingly, LYPcat is a classical PTP, but our structure does not contain the expected cyclic sulfenamide. Rather, catC227 is found in a disulfide bond with a back-door Cys, C129, a state previously only found in nonclassical PTPs. Another notable feature found in our protein shows that there is also another Cys found in the P-loop, potentially allowing for a secondary site to form a disulfide bond. To date, classical PTPs have not been shown to have a mode of redox regulation aside from the cyclic sulfenamide.

To get a better understanding of what might be happening during redox regulation of LYP, we created three mutants on C129 and C231, the two potential disulfide partners of the catC227: single point mutants C129S and C231S and a double mutant C129S-C231S. One of the initial concerns was whether the mutants still retained activity. We found that C129S has 48% of wild-type activity, while C231S and C129S-C231S both have 13% of wild-type activity (Figure 4A,C). The significantly reduced specific activity of C231S suggests its importance for catalysis. The double mutant, C129S-C231S, has similar specific activity to C231S, indicating that the additional C129S mutation does not significantly reduce the activity of the protein further. Thus, the effect of each separate mutation is not additive.

We then sought to understand the roles of each of the Cys in redox regulation of LYPcat. In T cells, rapid production of ROS

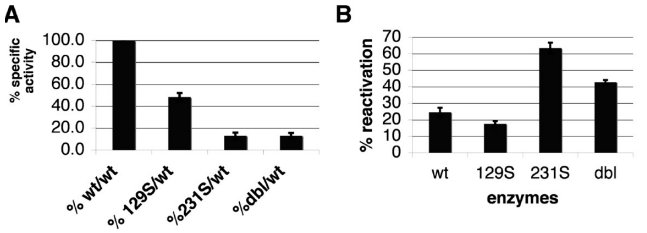


C

*Activity for hydrolysis of DiFMUP*

| Enzyme | % wt specific activity | % activity (inactivation) | % reactivation |
|---|---|---|---|
| wildtype LYPcat | 100.0 | --* | 24.6±2.7 |
| C129S | 48.2±3.9 | --* | 17.6±1.7 |
| C231S | 13.0±3.0 | --* | 63.4±3.3 |
| C129S-C231S | 13.1±2.6 | --* | 42.7±1.4 |

FIGURE 4: Phosphatase activity assays of LYP mutants. (A) Relative specific activity of each mutant protein compared to wild type using DiFMUP as the substrate. (B) Percent activity of the reactivated proteins ($H_2O_2$ treated, followed by DTT treatment) relative to its own protein's full activity before $H_2O_2$ inactivation. DiFMUP was used as the substrate. All reactivation percentages of the mutants were found to be statistically significantly different from that of the wild type using the paired *t* test. (C) Summary of the activity assay results using DiFMUP as the substrate. Column 1 lists each protein, column 2 gives the specific activity of each protein, column 3 gives the percent activity of each protein after inactivation by $H_2O_2$, and column 4 gives the reactivation activity as a percentage of each protein's original activity after 10 min of inactivation by $H_2O_2$, followed by DTT reactivation for 15 min. * No measurable activity.

is known to accompany TCR signaling (*41*−*43*). Recently, the tyrosine phosphatase SHP-2 has been reported to be regulated by ROS during TCR signaling (*44*). ROS may affect TCR signaling through regulation of the activity of LYP as well. In accordance, we added 100 $\mu$M $H_2O_2$ and incubated for 10 min with wild type and its mutants, finding that peroxide completely inactivated all of the proteins (Figure 4C). Oxidation of PTPs is known to sequester the catalytic Cys such that it cannot functionally work as a phosphatase. Across the PTP superfamily, it has been shown that various methods of protection for the catalytic Cys from highly oxidizing conditions allow for some reversibility under reducing conditions that can recover the active thiolate form of the catalytic Cys. To test whether this property is conserved in wild-type LYPcat and its mutants (Figure 4B,C), we attempted recovery of activity by incubating with 10 mM DTT for 15 min. The results showed that wild type recovers to about 25% of its original activity. Lack of 100% recovery was somewhat expected since reactivation kinetics by thiols is estimated to be 10−100 times slower than inactivation by $H_2O_2$ (*39*). Reactivation studies by Denu and Tanner (*39*) show that after 15 min VHR and PTP1 (rat) are only at about 20−25% of the maximal activation shown in their studies. In addition, since $H_2O_2$ is a strong oxidizer, some active centers may have been irreversibly oxidized, preventing 100% recovery. Interestingly, in the time over which the mutants were studied, percent reactivation in the C231S (63%) and C129S-C231S double mutant (43%) appeared to be significantly higher than in wild type (25%). However, the other single mutant, C129S, had a lower percent reactivation (18%) than wild type. The rate of catalysis of the reactivated samples remained constant over the time period measured (data not shown). Further, since the reactivation by DTT is continuous, even during measurement, we can conclude that reactivation is complete.

The reduction in reactivation of the C129S mutant after $H_2O_2$ treatment suggests that this residue is important in protecting catC227 from irreversible oxidation. Together with the structural data, these results suggest that at least one method of protection of LYP from ROS inactivation is through the disulfide bond between catC227 and the back-door C129. The C231S mutant, which shows a greater percent reactivation than wild type, still has the C129 available for disulfide bond formation, and the difference in reactivation between the C231S and C129S-C231S mutants can be similarly attributed to C129 availability for oxidation protection. Distances between the α carbon atoms of C129 and C227 in publicly available LYPcat structures (PDB codes 2P6X, 2QCT, 2QCJ) are 4.9−5.4 Å, and the distance in the disulfide-bonded structure is 5.6 Å, all of which are in the normal range (4.4−6.8 Å) of Cα−Cα distance of disulfide bonds (*26*). Thus, the disulfide bond between C129 and catC227 can be formed without any significant conformational change in the structure, involving just a rotation around $\chi_1$ for catC227.

While the role of C129 seems clear given previous studies on the back-door Cys, the role of C231 and its interaction with catC227 and C129 are not as straightforward. Given the higher reactivation rate of both C231S mutants, it appears that C231 suppresses reactivation in a reducing environment. One possibility is that C231 may be competing with C227 for reduction in the catalytic pocket. In the C231S mutant, catC227 would be free to be reduced, thus allowing LYPcat to recover activity even greater than that of the wild-type enzyme. Since a gain-of-function mutation of LYP has been linked to autoimmunity, it is possible that C231 evolved as a mechanism of negative regulation of LYP, which results in overall prevention of autoimmune diseases. Classical PTPs have previously demonstrated protection from oxidation through formation of a cyclic sulfenamide (*22*, *30*) between the catalytic Cys and the main-chain amide from the neighboring serine in the classical PTP signature motif HCSXGXGR[T/S]G, another factor that may affect reactivation rates.

## CONCLUDING REMARKS

LYP is a negative downstream regulator of T-cell signaling and a drug target for autoimmunity. In this report, we present a crystal structure of LYPcat involving an intramolecular disulfide bond with a phosphate bound in the catalytic pocket. We demonstrate that LYP, a classical PTP, forms this disulfide bond primarily with a back-door Cys, C129, in response to an oxidizing environment, a protective mechanism not previously seen in this class of PTPs. Surprisingly, C231 seems to play a role opposite to that of C129 in negatively regulating catalysis by inhibiting reactivation in a reducing environment. We propose that C129 and C231 comprise a yin-yang pair working as a built-in autoregulation circuit for this enzyme, playing a critical role in T-cell activation and autoimmunity.

## ACKNOWLEDGMENT

We thank Divya Krishnamurthy and Lauren Holden for enlightening experimental discussions and Tiffanie Nham for technical assistance in purification of the mutant proteins.

## REFERENCES

1. Hunter, T. (1987) A thousand and one protein kinases. *Cell 50*, 823–829.
2. Mustelin, T., Abraham, R. T., Rudd, C. E., Alonso, A., and Merlo, J. J. (2002) Protein tyrosine phosphorylation in T cell signaling. *Front. Biosci. 7*, d918–d969.

3. Mustelin, T., Feng, G. S., Bottini, N., Alonso, A., Kholod, N., Birle, D., Merlo, J., and Huynh, H. (2002) Protein tyrosine phosphatases. *Front. Biosci. 7*, d85–d142.
4. Fischer, E. H., Charbonneau, H., and Tonks, N. K. (1991) Protein tyrosine phosphatases: a diverse family of intracellular and transmembrane enzymes. *Science (New York) 253*, 401–406.
5. Mustelin, T., and Taskén, K. (2003) Positive and negative regulation of T-cell activation through kinases and phosphatases. *Biochem. J. 371*, 15–27.
6. Tonks, N. K., and Neel, B. G. (1996) From form to function: signaling by protein tyrosine phosphatases. *Cell 87*, 365–368.
7. Walton, K. M., and Dixon, J. E. (1993) Protein tyrosine phosphatases. *Annu. Rev. Biochem. 62*, 101–120.
8. Alonso, A., Sasin, J., Bottini, N., Friedberg, I., Osterman, A., Godzik, A., Hunter, T., Dixon, J., and Mustelin, T. (2004) Protein tyrosine phosphatases in the human genome. *Cell 117*, 699–711.
9. Andersen, J. N., Mortensen, O. H., Peters, G. H., Drake, P. G., Iversen, L. F., Olsen, O. H., Jansen, P. G., Andersen, H. S., Tonks, N. K., and Møller, N. P. (2001) Structural and evolutionary relationships among protein tyrosine phosphatase domains. *Mol. Cell. Biol. 21*, 7117–7136.
10. Bottini, N., Bottini, E., Gloria-Bottini, F., and Mustelin, T. (2002) Low-molecular-weight protein tyrosine phosphatase and human disease: in search of biochemical mechanisms. *Arch. Immunol. Exp. Ther. 50*, 95–104.
11. Bottini, N., Musumeci, L., Alonso, A., Rahmouni, S., Nika, K., Rostamkhani, M., MacMurray, J., Meloni, G. F., Lucarelli, P., Pellecchia, M., Eisenbarth, G. S., Comings, D., and Mustelin, T. (2004) A functional variant of lymphoid tyrosine phosphatase is associated with type I diabetes. *Nat. Genet. 36*, 337–338.
12. Buhrman, G., Parker, B., Sohn, J., Rudolph, J., and Mattos, C. (2005) Structural mechanism of oxidative regulation of the phosphatase Cdc25B via an intramolecular disulfide bond. *Biochemistry 44*, 5307–5316.
13. Kozlov, G., Cheng, J., Ziomek, E., Banville, D., Gehring, K., and Ekiel, I. (2004) Structural insights into molecular function of the metastasis-associated phosphatase PRL-3. *J. Biol. Chem. 279* 11882–11889.
14. Tonks, N. K., and Neel, B. G. (2001) Combinatorial control of the specificity of protein tyrosine phosphatases. *Curr. Opin. Cell Biol. 13*, 182–195.
15. Wang, Z., Shen, D., Parsons, D. W., Bardelli, A., Sager, J., Szabo, S., Ptak, J., Silliman, N., Peters, B. A., van der Heijden, M. S., Parmigiani, G., Yan, H., Wang, T. L., Riggins, G., Powell, S. M., Willson, J. K., Markowitz, S., Kinzler, K. W., Vogelstein, B., and Velculescu, V. E. (2004) Mutational analysis of the tyrosine phosphatome in colorectal cancers. *Science (New York) 304*, 1164–1166.
16. Wu, H., Cantor, R. M., Graham, D. S., Lingren, C. M., Farwell, L., Jager, P. L., Bottini, N., Grossman, J. M., Wallace, D. J., Hahn, B. H., Julkunen, H., Hebert, L. A., Rovin, B. H., Birmingham, D. J., Rioux, J. D., Yu, C. Y., Kere, J., Vyse, T. J., and Tsao, B. P. (2005) Association analysis of the R620W polymorphism of protein tyrosine phosphatase PTPN22 in systemic lupus erythematosus families: increased T allele frequency in systemic lupus erythematosus patients with autoimmune thyroid disease. *Arthritis Rheum. 52* 2396–2402.
17. Cloutier, J. F., and Veillette, A. (1999) Cooperative inhibition of T-cell antigen receptor signaling by a complex between a kinase and a phosphatase. *J. Exp. Med. 189*, 111–121.
18. Begovich, A. B., Carlton, V. E., Honigberg, L. A., Schrodi, S. J., Chokkalingam, A. P., Alexander, H. C., Ardlie, K. G., Huang, Q., Smith, A. M., Spoerke, J. M., Conn, M. T., Chang, M., Chang, S. Y., Saiki, R. K., Catanese, J. J., Leong, D. U., Garcia, V. E., McAllister, L. B., Jeffery, D. A., Lee, A. T., Batliwalla, F., Remmers, E., Criswell, L. A., Seldin, M. F., Kastner, D. L., Amos, C. I., Sninsky, J. J., and Gregersen, P. K. (2004) A missense single-nucleotide polymorphism in a gene encoding a protein tyrosine phosphatase (PTPN22) is associated with rheumatoid arthritis. *Am. J. Hum. Genet. 75* 330–337.
19. Kyogoku, C., Langefeld, C. D., Ortmann, W. A., Lee, A., Selby, S., Carlton, V. E., Chang, M., Ramos, P., Baechler, E. C., Batliwalla, F. M., Novitzke, J., Williams, A. H., Gillett, C., Rodine, P., Graham, R. R., Ardlie, K. G., Gaffney, P. M., Moser, K. L., Petri, M., Begovich, A. B., Gregersen, P. K., and Behrens, T. W. (2004) Genetic association of the R620W polymorphism of protein tyrosine phosphatase PTPN22 with human SLE. *Am. J. Hum. Genet. 75*, 504–507.
20. Vang, T., Congia, M., Macis, M. D., Musumeci, L., Orrú, V., Zavattari, P., Nika, K., Tautz, L., Taskén, K., Cucca, F., Mustelin, T., and Bottini, N. (2005) Autoimmune-associated lymphoid tyrosine phosphatase is a gain-of-function variant. *Nat. Genet. 37*, 1317–1319.
21. den Hertog, J., Groen, A., and van der Wijk, T. (2005) Redox regulation of protein-tyrosine phosphatases. *Arch. Biochem. Biophys. 434*, 11–15.
22. Groen, A., Lemeer, S., van der Wijk, T., Overvoorde, J., Heck, A. J., Ostman, A., Barford, D., Slijper, M., and den Hertog, J. (2005) Differential oxidation of protein-tyrosine phosphatases. *J. Biol. Chem. 280*, 10298–10304.
23. Caselli, A., Marzocchini, R., Camici, G., Manao, G., Moneti, G., Pieraccini, G., and Ramponi, G. (1998) The inactivation mechanism of low molecular weight phosphotyrosine-protein phosphatase by H2O2. *J. Biol. Chem. 273*, 32554–32560.
24. Xing, K., Raza, A., Löfgren, S., Fernando, M. R., Ho, Y. S., and Lou, M. F. (2007) Low molecular weight protein tyrosine phosphatase (LMW-PTP) and its possible physiological functions of redox signaling in the eye lens. *Biochim. Biophys. Acta 1774* 545–555.
25. Chiarugi, P., Fiaschi, T., Taddei, M. L., Talini, D., Giannoni, E., Raugei, G., and Ramponi, G. (2001) Two vicinal cysteines confer a peculiar redox regulation to low molecular weight protein tyrosine phosphatase in response to platelet-derived growth factor receptor stimulation. *J. Biol. Chem. 276*, 33478–33487.
26. Cho, S. H., Lee, C. H., Ahn, Y., Kim, H., Ahn, C. Y., Yang, K. S., and Lee, S. R. (2004) Redox regulation of PTEN and protein tyrosine phosphatases in H(2)O(2) mediated cell signaling. *FEBS Lett. 560* 7–13.
27. Fauman, E. B., Cogswell, J. P., Lovejoy, B., Rocque, W. J., Holmes, W., Montana, V. G., Piwnica-Worms, H., Rink, M. J., and Saper, M. A. (1998) Crystal structure of the catalytic domain of the human cell cycle control phosphatase, Cdc25A. *Cell 93*, 617–625.
28. Lee, S. R., Yang, K. S., Kwon, J., Lee, C., Jeong, W., and Rhee, S. G. (2002) Reversible inactivation of the tumor suppressor PTEN by $H_2O_2$. *J. Biol. Chem. 277*, 20336–20342.
29. Sohn, J., and Rudolph, J. (2003) Catalytic and chemical competence of regulation of cdc25 phosphatase by oxidation/reduction. *Biochemistry 42*, 10060–10070.
30. Salmeen, A., Andersen, J. N., Myers, M. P., Meng, T. C., Hinks, J. A., Tonks, N. K., and Barford, D. (2003) Redox regulation of protein tyrosine phosphatase 1B involves a sulphenyl-amide intermediate. *Nature 423*, 769–773.
31. van Montfort, R. L., Congreve, M., Tisi, D., Carr, R., and Jhoti, H. (2003) Oxidation state of the active-site cysteine in protein tyrosine phosphatase 1B. *Nature 423*, 773–777.
32. The CCP4 Suite (1994) Programs for protein crystallography. *Acta Crystallogr., Sect. D: Biol. Crystallogr. 50*, 760–763.
33. Yu, X., Sun, J. P., He, Y., Guo, X., Liu, S., Zhou, B., Hudmon, A., and Zhang, Z. Y. (2007) Structure, inhibitor, and regulatory mechanism of Lyp, a lymphoid-specific tyrosine phosphatase implicated in autoimmune diseases. *Proc. Natl. Acad. Sci. U.S.A. 104*, 19767–19772.
34. Barr, A. J., Ugochukwu, E., Lee, W. H., King, O. N., Filippakopoulos, P., Alfano, I., Savitsky, P., Burgess-Brown, N. A., Muller, S., and Knapp, S. (2009) Large-scale structural analysis of the classical human protein tyrosine phosphatome. *Cell 136*, 352–363.
35. Gruninger, R. J., Brent Selinger, L., and Mosimann, S. C. (2008) Effect of ionic strength and oxidation on the P-loop conformation of the protein tyrosine phosphatase-like phytase, PhyAsr. *FEBS J. 275*, 3783–3792.
36. Reynolds, R. A., Yem, A. W., Wolfe, C. L., Deibel, M. R., Chidester, C. G., and Watenpaugh, K. D. (1999) Crystal structure of the catalytic subunit of Cdc25B required for G2/M phase transition of the cell cycle. *J. Mol. Biol. 293*, 559–568.
37. Denu, J. M., and Dixon, J. E. (1998) Protein tyrosine phosphatases: mechanisms of catalysis and regulation. *Curr. Opin. Chem. Biol. 2*, 633–641.
38. Yang, J., Groen, A., Lemeer, S., Jans, A., Slijper, M., Roe, S. M., den Hertog, J., and Barford, D. (2007) Reversible oxidation of the membrane distal domain of receptor PTPalpha is mediated by a cyclic sulfenamide. *Biochemistry 46*, 709–719.
39. Denu, J. M., and Tanner, K. G. (1998) Specific and reversible inactivation of protein tyrosine phosphatases by hydrogen peroxide: evidence for a sulfenic acid intermediate and implications for redox regulation. *Biochemistry 37*, 5633–5642.
40. Sun, J. P., Wang, W. Q., Yang, H., Liu, S., Liang, F., Fedorov, A. A., Almo, S. C., and Zhang, Z. Y. (2005) Structure and biochemical properties of PRL-1, a phosphatase implicated in cell growth, differentiation, and tumor invasion. *Biochemistry 44*, 12009–12021.

41. Salmeen, A., and Barford, D. (2005) Functions and mechanisms of redox regulation of cysteine-based phosphatases. *Antioxid. Redox Signal. 7*, 560–577.
42. Meng, T. C., Buckley, D. A., Galic, S., Tiganis, T., and Tonks, N. K. (2004) Regulation of insulin signaling through reversible oxidation of the protein-tyrosine phosphatases TC45 and PTP1B. *J. Biol. Chem. 279*, 37716–37725.
43. Yamamura, H. (2002) Redox control of protein tyrosine phosphorylation. *Antioxid. Redox Signal. 4*, 479–480.
44. Kwon, J., Qu, C. K., Maeng, J. S., Falahati, R., Lee, C., and Williams, M. S. (2005) Receptor-stimulated oxidation of SHP-2 promotes T-cell adhesion through SLP-76-ADAP. *EMBO J. 24*, 2331–2341.